Supporting Information

Intrinsic Role of Molecular Architectonics in Enhancing the Catalytic Activity of Lead in Glucose Hydrolysis

Bappaditya Roy, Satyajit Pal, and Thimmaiah Govindaraju*

Bioorganic Chemistry Laboratory, New Chemistry Unit and School of Advanced Materials (SAMat), Jawaharlal Nehru Centre for Advanced Scientific Research, Jakkur P.O., Bengaluru 560064, Karnataka, India.

Corresponding Author (T.G.): *tgraju@jncasr.ac.in*

Contents

1. Materials and methods

Materials. Reagent grade chemicals and solvents were purchased from Merck, India and TCI India, and used without any further purification unless mentioned. The solvents were brought as HPLC grade from Spectrochem, India. Deuterated solvents were purchased from Eurisotop. Anhydrous sodium hydroxide (>99%), sodium acetate (>99%) and mono and disaccharides (>99%) were procured from Merck, India and vacuum dried before its use for experiments. Minisart Syringe Filter, Surfactant-free Cellulose Acetate (SFCA), Pore Size 0.2 μm was brought from Sartorius Stedim biotech. For experiments, we have used purified water collected form TKA GenPure Germany.

Methods. Absorbance spectra were recorded on Perkin Elmer Model Lambda 900 spectrophotometer. The spectra were recorded in quartz cuvettes of either 2 or 10 mm path lengths. Fluorescence spectra were recorded on a PerkinElmer model LS 55 spectrophotometer. All fluorescence emission spectra were recorded with excitation wavelength λ_{ex} = 350 nm and analyzed in quartz cuvette of 10 mm path length. Nuclear magnetic resonance spectra (^{1}H NMR and ^{13}C NMR) were recorded on a Bruker AV-400 and JEOL 600 spectrometer with chemical shifts are reported as ppm in deuterated solvents with tetramethylsilane (TMS) as internal standard. Fourier-transform infrared spectroscopy (FTIR) spectra were recorded on a Bruker IFS 66/V spectrometer using KBr pellet. The measurements were done for the thin film sample on a glass surface and vacuum-dried at laboratory temperature. Mass spectra were acquired on Agilent 6538 UHD HRMS/Q-TOF high resolution, Shimadzu LCMS-2020, and Bruker Autoflex Speed MALDI-TOF spectrometer. Powder X-ray diffraction (PXRD) patterns were recorded with a Rigaku-99 (Miniflex) diffractometer using Cu Kα radiation (λ = 1.5406 Å). The samples were prepared by drop-casting onto a clean quartz substrate and allowed to dry in air followed by vacuum drying for 1 day at room temperature. X-ray photoelectron spectroscopy (XPS) measurements were performed on as-prepared samples drop-casted on silicon wafer, using Al Ka radiation (1486.6 eV) in a commercial photoelectron spectrometer from VSW Scientific Instruments. The hydrodynamic sizes of the assembly-architectures were determined using dynamic light scattering measurements (DLS). Size measurement was performed in ZetaPALS, Zeta Potential Analyzer (Brookhaven Instruments Corporation, USA). Transmission electron microscopy (TEM) analysis was performed in JEOL 1230 TEM with a Hamamatsu ORCA

camera at an accelerating voltage of 120 kV. Digital images of the vials containing solution of metal complexes were taken in Canon SX50HX digital camera. All the raw data was processed and analyzed in Origin 8.5 software.

Preparation of stock solutions. All the amphiphile samples were weighed in a digital balance (Sartorius India Pvt. Ltd.) and taken calculated amount into a 10.0 mL glass vial to prepare an 8.0 mM stock solution in DMSO. 20 mM $Pb(NO_3)_2$ stock solution was prepared in water. 0.5 N NaOH and 0.5 N HCl stocks were prepared in water for maintaining the pH of the solutions. The mono and disaccharide stock solutions were prepared fresh 100.0 mM in water each time before the experiments.

2. Synthesis and characterization

The rationally designed *D*-gluconamide amphiphiles were synthesized by conjugating hydrophilic *D*-gluconic acid with different alkyl or aromatic amines as hydrophobic units (Figure S1).[1-4]

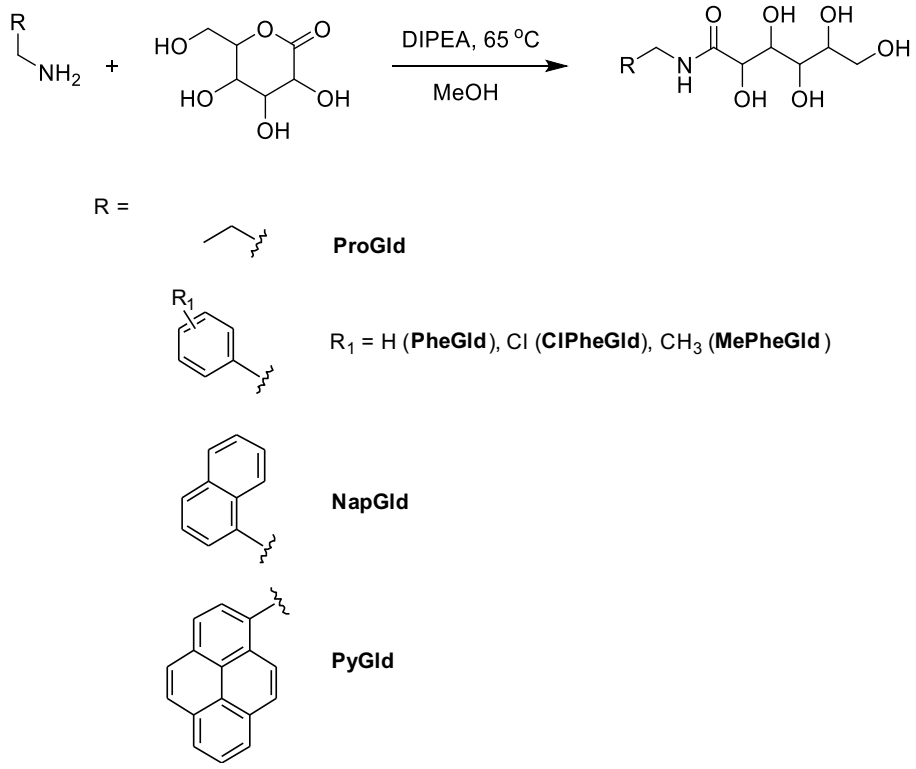

Figure S1. General scheme for synthesis of *N*-alkyl or aryl−*D*−gluconamides.

(a) General procedure for synthesis of *N*−alkyl or aryl−*D*−gluconamides.

To a stirred solution of the desired amine (1.0 equiv) in methanol (MeOH, 20 mL), *N,N*-diisopropylethylamine (DIPEA, 10 equiv) was added and stirred for 15 min followed by the addition of *D*-gluconic acid-*δ*-lactone (3.5 equiv). The reaction mixture was then refluxed for 12 h at 70 ºC temperature under stirring conditions. After completion of the reaction, the reaction mixture was evaporated under vacuum to obtain white solid powder which was further recrystallized in ethanol to obtain the final product.

Characterization of the Amphiphiles.

(a) *N*−Propyl−*D*−gluconamide (**ProGld**)

Yield: 64%. ^{1}H NMR (400 MHz, DMSO-d_6): δ 7.58 (t, J = 5.9 Hz, 1H), 5.34 (d, J = 5.1 Hz, 1H), 4.52 (d, J = 5.0 Hz, 1H), 4.46 (d, J = 5.4 Hz, 1H), 4.38 (d, J = 7.2 Hz, 1H), 4.32 (t, J = 5.7 Hz, 1H), 3.99 – 3.94 (m, 1H), 3.89 (s, 1H), 3.56 (s, 1H), 3.47 (s, 2H), 3.37 (dt, J = 11.0, 5.6 Hz, 1H), 1.44 – 1.35 (m, 2H), 1.27 (dq, J = 14.1, 7.1 Hz, 2H), 0.86 (t, J = 7.3 Hz, 3H). ^{13}C NMR (100 MHz, DMSO-d_6): δ 172.2, 73.6, 72.4, 71.5, 70.1, 63.3, 37.9, 31.2, 19.5, 13.7. HRMS (ESI) (*m/z*): Calcd. 251.1369 for $C_{10}H_{21}NO_6$; Found 252.1497, $[M+H]^+$.

(b) *N*−Benzyl−*D*−gluconamide (**PheGld**):

Yield: 75%. ^{1}H NMR (400 MHz, DMSO-d_6): δ = 8.15 (t, J = 6.2 Hz, 1H), 7.30 (dd, J = 7.6, 5.6 Hz, 4H), 7.25 – 7.18 (m, 1H), 5.44 (d, J = 5.1 Hz, 1H), 4.56 (d, J = 5.1 Hz, 1H), 4.50 (d, J = 5.5 Hz, 1H), 4.45 (d, J = 7.2 Hz, 1H), 4.33 (dd, J = 13.0, 6.0 Hz, 3H), 4.09 – 4.05 (m, 1H), 3.97 (d, J = 5.2 Hz, 1H), 3.58 (dd, J = 12.0, 7.1 Hz, 1H), 3.50 (s, 2H), 3.38 (dt, J = 11.1, 5.6 Hz, 1H). ^{13}C NMR (100 MHz, DMSO-d_6): δ 172.5, 139.5, 128.1, 127.1, 126.5, 73.7, 72.48, 71.5, 70.1, 63.3, 41.7. HRMS (ESI) (*m/z*): Calculated 285.1212 for $C_{13}H_{19}NO_6$; found 286.1347, $[M+H]^+$.

(c) *N*−Methylbenzyl−*D*−gluconamide (**MePheGld**)

Yield: 76%. ^{1}H NMR (400 MHz, DMSO-d_6): δ 8.09 (t, J = 6.2 Hz, 1H), 7.16 (d, J = 7.9 Hz, 2H), 7.09 (d, J = 7.9 Hz, 2H), 5.43 (d, J = 5.1 Hz, 1H), 4.55 (s, 1H), 4.50 (s, 1H), 4.45 (d, J = 7.3 Hz, 1H), 4.34 (t, J = 5.7 Hz, 1H), 4.26 (d, J = 6.3 Hz, 2H), 4.08 – 4.02 (m, 1H), 3.95 (s, 1H), 3.58 (s, 1H), 3.49 (s, 2H), 3.37 (dt, J = 11.0, 5.6 Hz, 1H), 2.26 (s, 3H). ^{13}C NMR (100 MHz, DMSO-d_6): δ 172.5, 136.5, 135.6, 128.7, 127.2, 73.8, 72.5, 71.5, 70.1, 63.4, 41.5, 39.5, 20.7. HRMS (ESI) (*m/z*): Calculated 299.1369 for $C_{14}H_{21}NO_6$; found 300.1158, $[M+H]^+$.

(d) *N*−Chlorobenzyl−*D*−gluconamide (**ClPheGld**)

Yield: 72%. ^{1}H NMR (400 MHz, DMSO-d_6): δ 8.23 (t, J = 6.3 Hz, 1H), 7.32 (q, J = 8.6 Hz, 4H), 5.45 (d, J = 5.0 Hz, 1H), 4.55 (d, J = 5.2 Hz, 1H), 4.50 (d, J = 5.6 Hz, 1H), 4.45 (d, J = 7.2 Hz, 1H), 4.33 (t, J = 5.7 Hz, 1H), 4.31 – 4.26 (m, 2H), 4.09 – 4.04 (m, 1H), 3.96 (d, J = 12.4 Hz, 1H), 3.58 (d, J = 18.9 Hz, 1H), 3.50 (s, 2H), 3.38 (dt, J = 11.0, 5.6 Hz, 1H). ^{13}C NMR (100 MHz,

DMSO-d_6): δ 172.7, 138.70, 131.1, 129.0, 129.0, 73.8, 72.4, 71.5, 70.2, 63.3, 41.1, 39.5. HRMS (ESI) (*m/z*): Calculated 319.0823 for $C_{13}H_{18}ClNO_6$; found 320.0654, $[M+H]^+$.

(e) *N*−Naphthylmethyl−*D*−gluconamide (**NapGld**)

Yield = 82%. ^{1}H NMR (400 MHz, DMSO-d_6): δ 8.16 (t, J = 6.0 Hz, 1H), 8.11 (d, J = 7.4 Hz, 1H), 7.94 (d, J = 9.4 Hz, 1H), 7.83 (d, J = 8.0 Hz, 1H), 7.61 – 7.41 (m, 4H), 5.48 (d, J = 5.1 Hz, 1H), 4.85 – 4.70 (m, 2H), 4.57 (d, J = 4.6 Hz, 1H), 4.51 (dd, J = 13.1, 6.1 Hz, 2H), 4.35 (t, J = 5.6 Hz, 1H), 4.14 – 4.08 (m, 1H), 4.00 (s, 1H), 3.60 (d, J = 13.3 Hz, 1H), 3.52 (s, 2H), 3.39 (dt, J = 10.8, 5.5 Hz, 1H). ^{13}C NMR (100 MHz, DMSO-d_6): δ 172.5, 134.5, 133.2, 130.7, 128.4, 127.2, 126.2, 125.7, 125.4, 124.9, 123.4, 73.8, 72.5, 71.6, 70.2, 63.4. HRMS (ESI) (*m/z*): Calculated 335.1369 for $C_{17}H_{21}NO_6$, found 336.1513, $[M+H]^+$.

(f) *N*−Pyrenemethyl−*D*−gluconamide (**PyGld**)

Yield = 88%. ^{1}H NMR (400 MHz, DMSO-d_6): δ 8.44 (d, J = 9.3 Hz, 1H), 8.36 (t, J = 6.0 Hz, 1H), 8.30 (t, J = 7.3 Hz, 2H), 8.25 (d, J = 7.9 Hz, 2H), 8.16 (s, 2H), 8.09 (dd, J = 15.7, 7.9 Hz, 2H), 5.49 (d, J = 5.1 Hz, 1H), 5.13 – 5.00 (m, 2H), 4.57 (d, J = 5.1 Hz, 1H), 4.52 (dd, J = 9.7, 6.3 Hz, 2H), 4.35 (t, J = 5.7 Hz, 1H), 4.17 – 4.12 (m, 1H), 4.06 – 4.01 (m, 1H), 3.61 (dd, J = 13.9, 6.1 Hz, 1H), 3.53 (dd, J = 17.2, 8.1 Hz, 2H), 3.40 (dt, J = 10.9, 5.6 Hz, 1H). ^{13}C NMR (100 MHz, DMSO-d_6): δ 172.6, 132.9, 130.8, 130.3, 129.9, 127.8, 127.4, 126.9, 126.2, 125.1, 124.7, 123.9, 123.2, 73.9, 72.5, 71.6, 70.3, 63.4. HRMS (ESI) (*m/z*): Calculated 409.1525 for $C_{23}H_{23}NO_6$; found 410.7222, $[M+H]^+$.

^{1}H NMR spectrum of **ProGld**

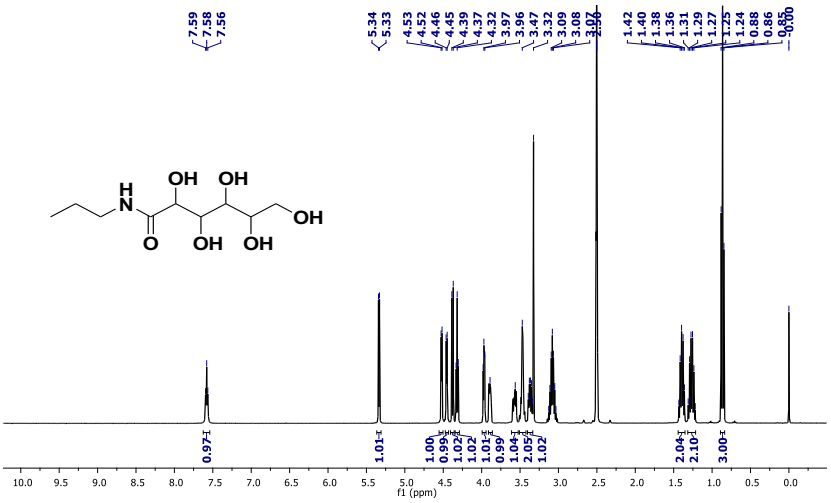

^{13}C NMR spectrum of **ProGld**

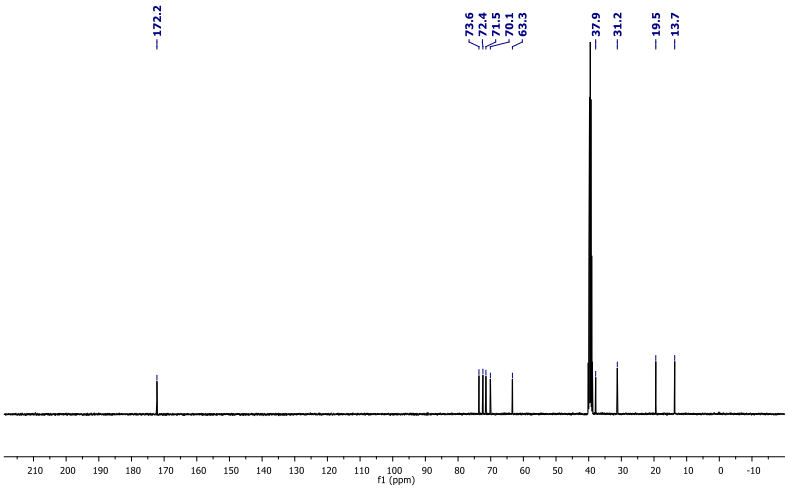

HRMS-ESI spectrum of **ProGld**

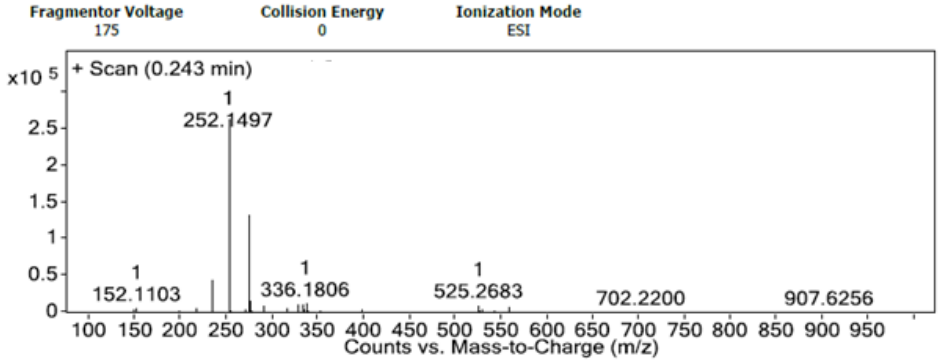

^{1}H NMR spectrum of **PheGld**

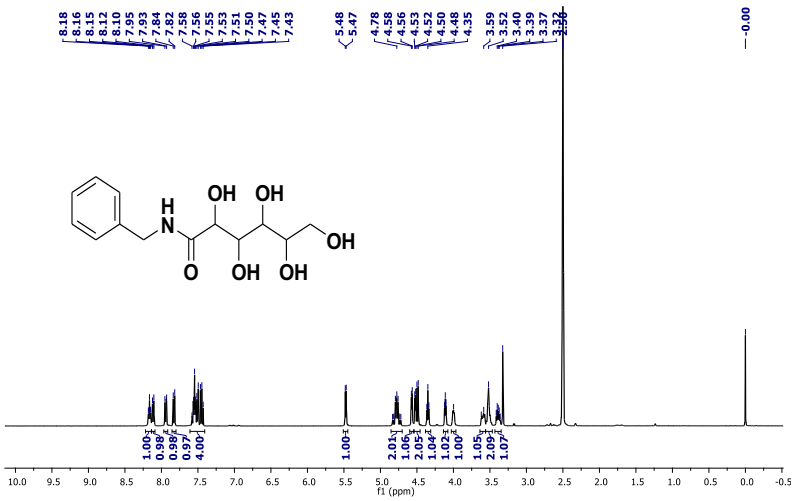

^{13}C NMR spectrum of **PheGld**

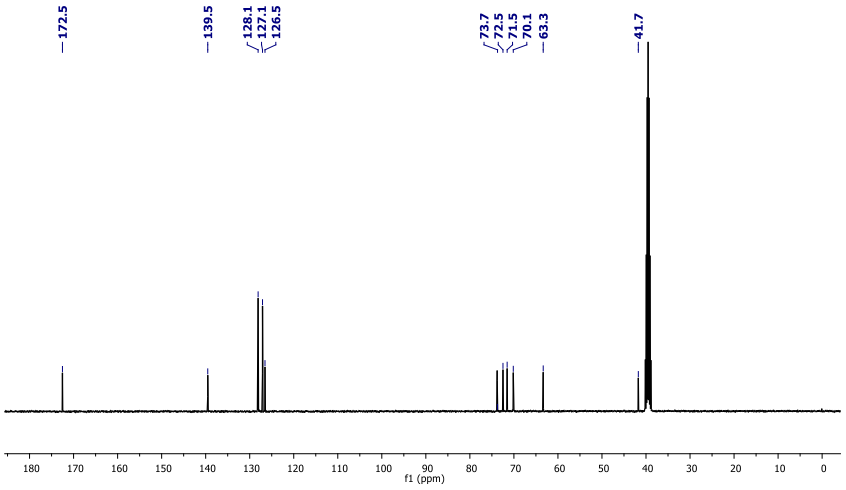

HRMS-ESI spectrum of **PheGld**

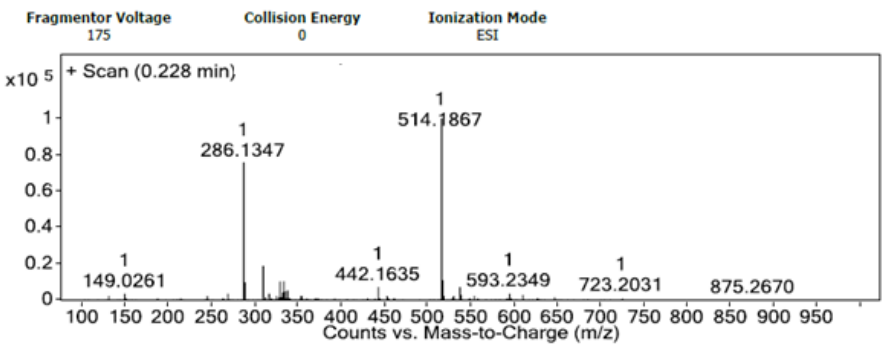

^{1}H NMR spectrum of **MePheGld**

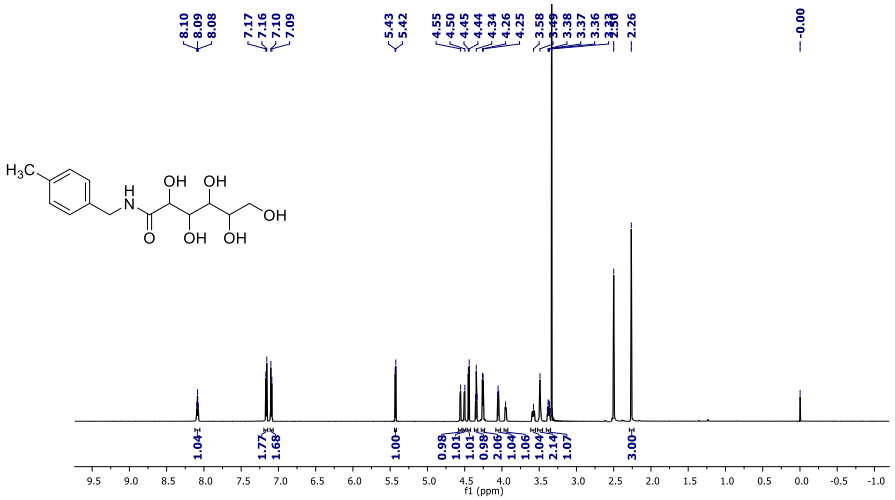

^{13}C NMR spectrum of **MePheGld**

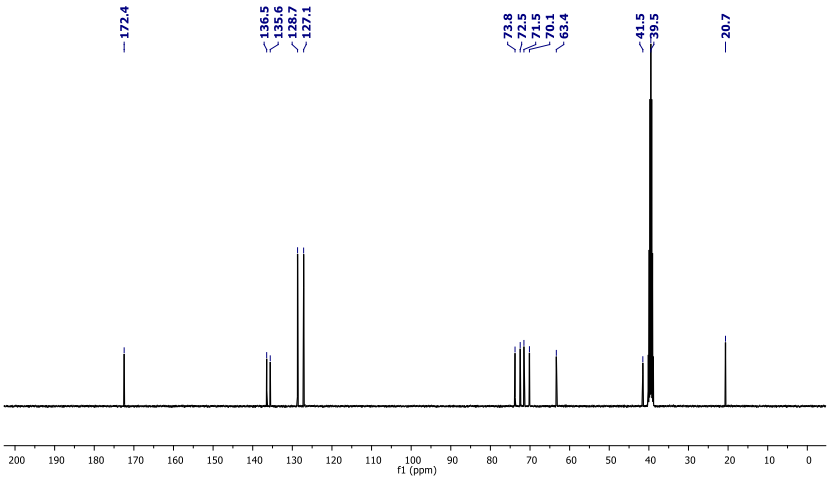

HRMS-ESI spectrum of **MePheGld**

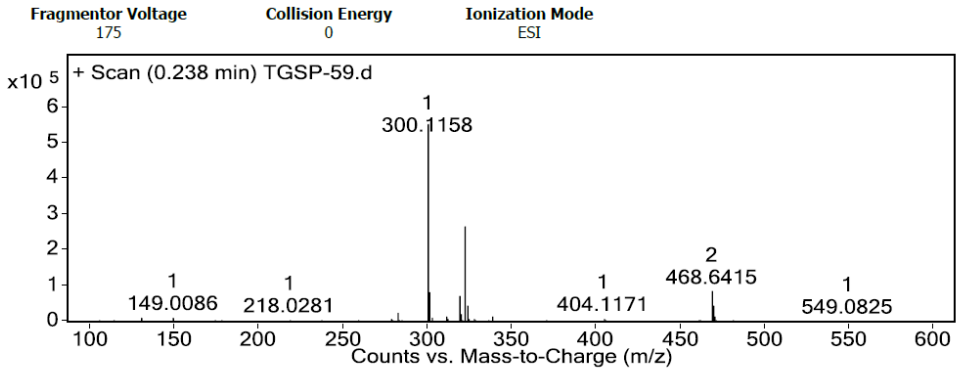

^{1}H NMR spectrum of **ClPheGld**

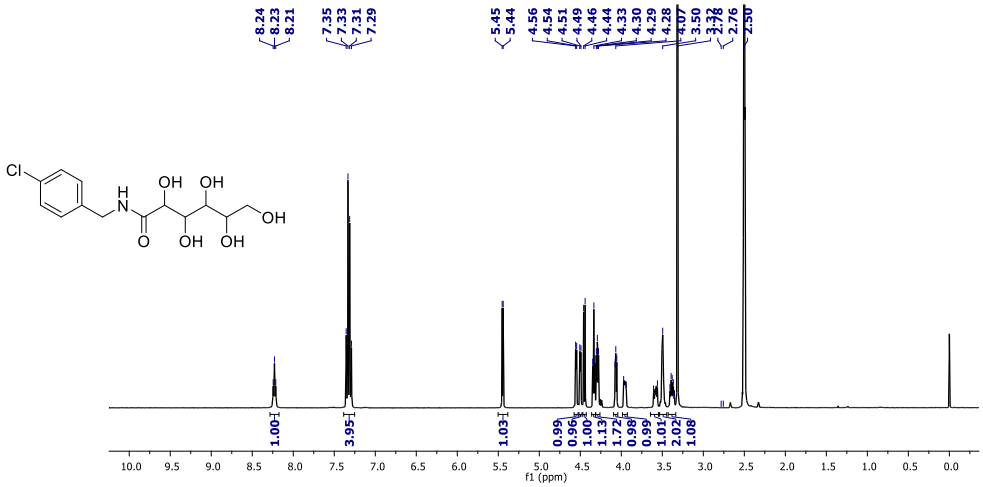

^{13}C NMR spectrum of **ClPheGld**

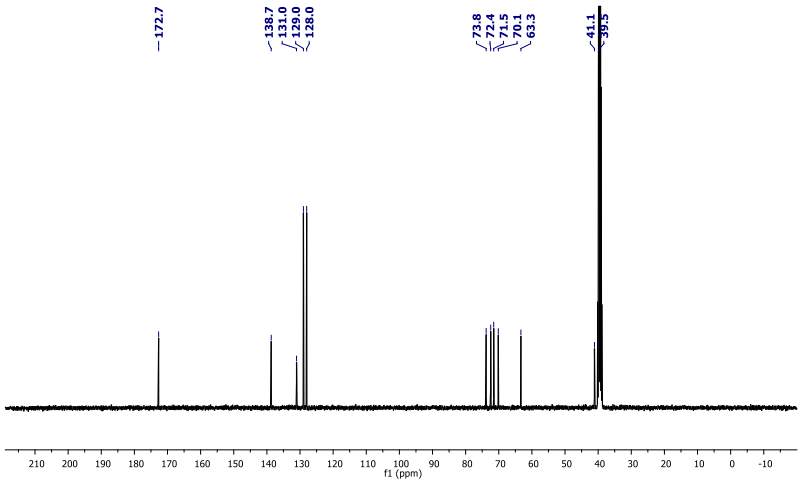

HRMS-ESI spectrum of **ClPheGld**

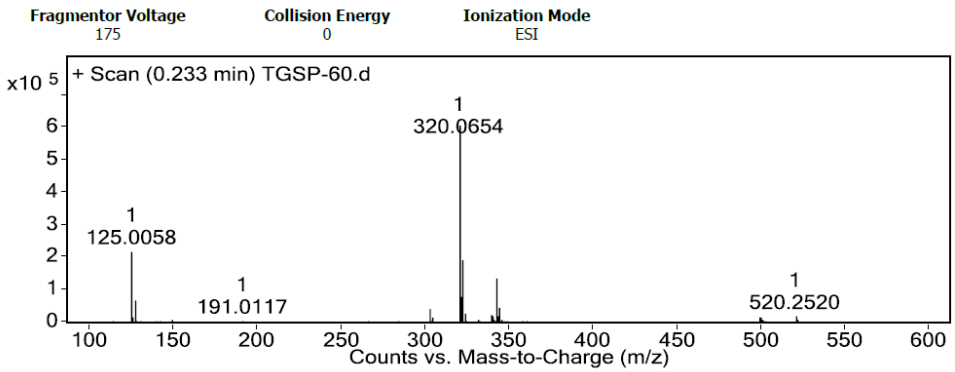

^{1}H NMR spectrum of **NapGld**

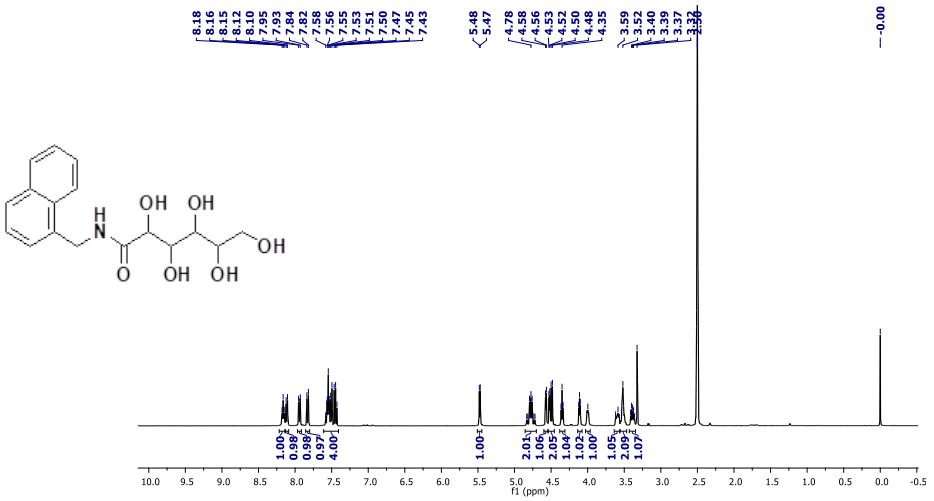

^{13}C NMR spectrum of **NapGld**

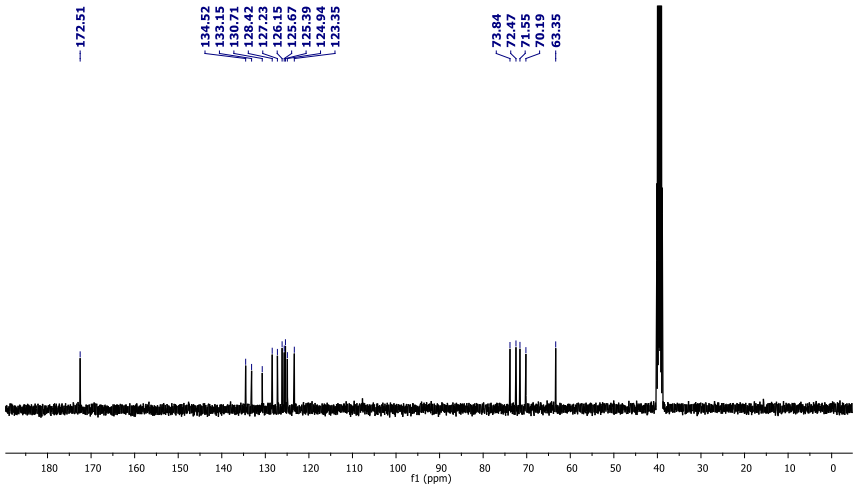

HRMS-ESI spectrum of **NapGld**

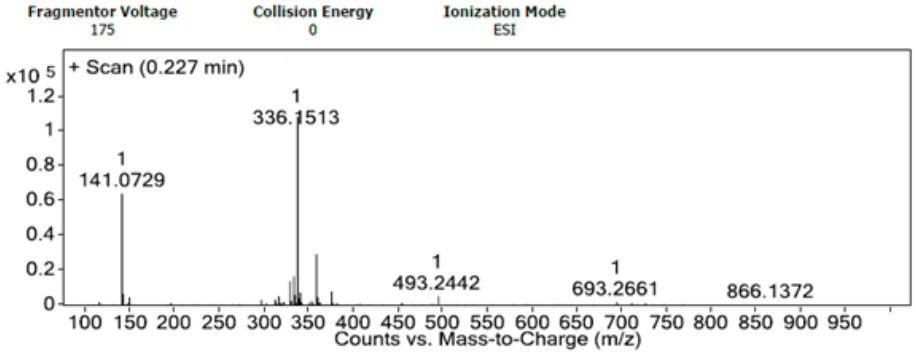

^{1}H NMR spectrum of **PyGld**

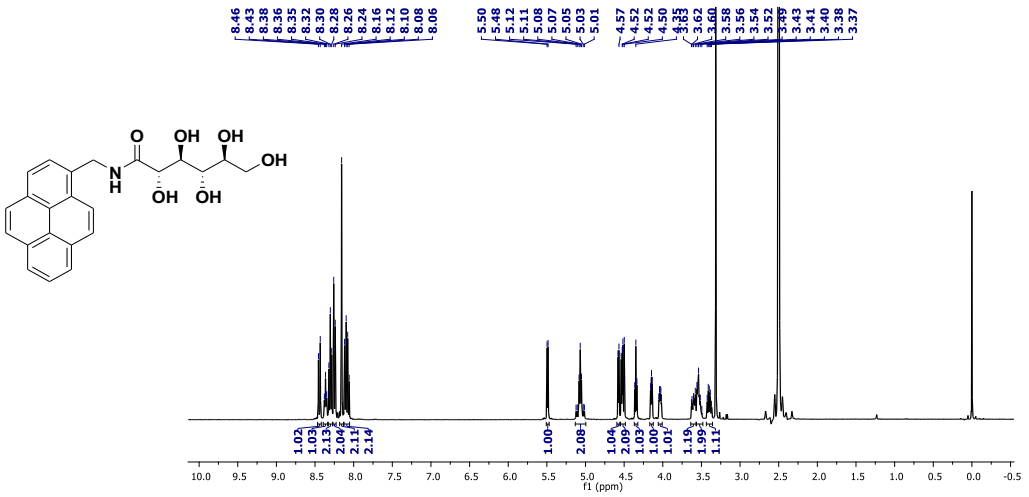

^{13}C NMR spectrum of **PyGld**

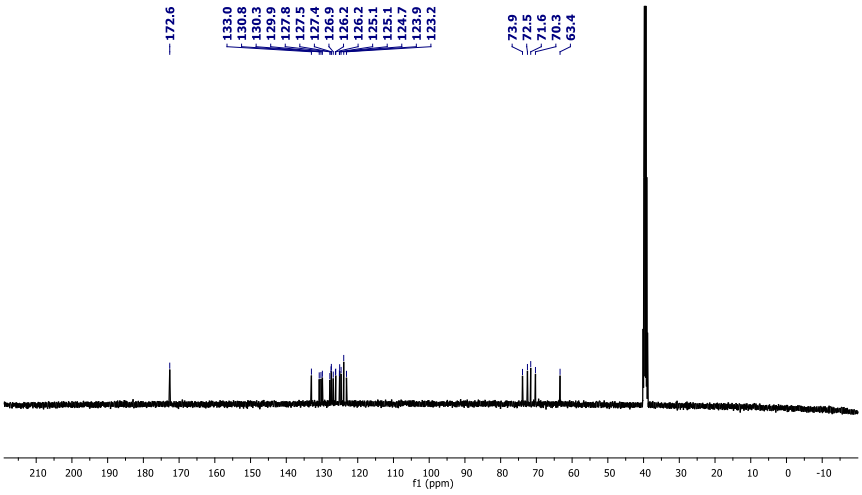

HRMS-ESI spectrum of **PyGld**

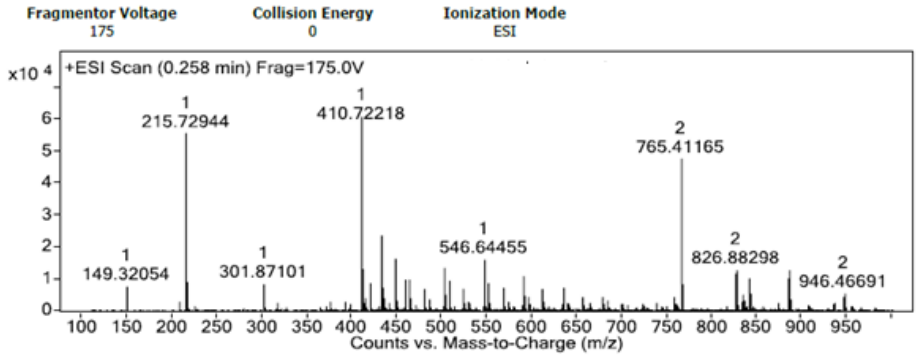

3. Experimental section

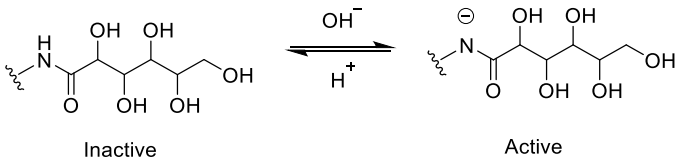

Figure S2. Activation and deactivation of amide –**NH**−CO– bond in the presence and absence of chemical stimuli (acidic/basic pH).

(a) Metal binding study.

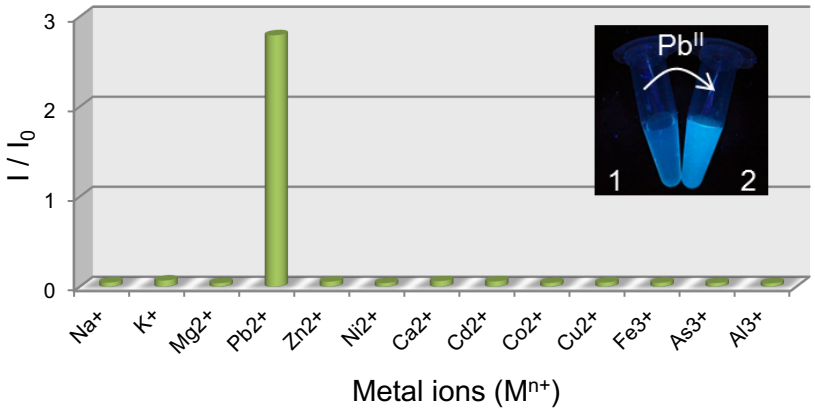

Figure S3. Metal ion selectivity of **PyGld** at 50 μM concentration in 5%(*v*/*v*) DMSO−water at pH 12.2 and 22 ºC. Metal salt concentration was used is 500 μM. Inset: Photographs of the vials (1 and 2) containing **PyGld** and **PyGld**−Pb^{II} solutions under the UV-lamp (365 nm).

(b) Fluorescence study for gluconamide−Pb^{II} complex

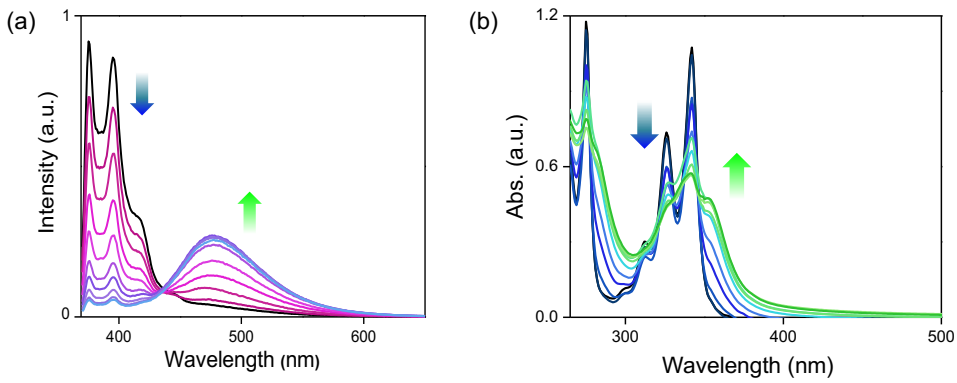

Figure S4. Ratiometric fluorescence (a) and absorbance (b) spectral change of **PyGld** (50 μM) with the increasing concentration of Pb^{II} (25–600 μM) at pH = 12.2 of 5%(*v*/*v*) DMSO−water and at 22 °C.

(c) **^{1}H NMR Study.** The Pb^{II} binding interaction with **PyGld** was investigated in ^{1}H NMR experiment at pH ~7.0 (D_2O) upon addition of 12.2 μL (0.5 mM NaOD) and in the presence of different Pb^{II} concentrations. Standard solutions of 1.0 mM **PyGld** in DMSO−d_6 and 100 mM $Pb(NO_3)_2$ in D_2O were prepared. ^{1}H NMR of **PyGld** at 250 μM concentration (125 μL) in 5%(*v*/*v*) water−DMSO-d_6 (pH ~7.0) solvent system was measured. Then 125 μL of **PyGld** standard solution was diluted to 358.75 μL by adding 10 μL 0.5 mM NaOD in D_2O in order to set the desired pH ~12. The change in ^{1}H NMR spectra was then recorded in the presence of Pb^{II} at pH ~12. Pb^{II} concentration was varied from 250 to 750 μM.

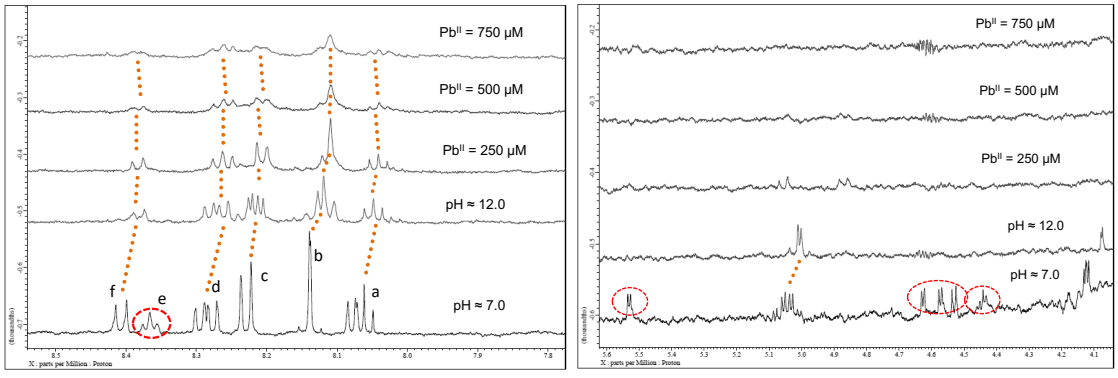

Figure S5. ^{1}H NMR spectra of amphiphile **PyGld** in different conditions – (i) at pH ~7.0 and ~12.0 and (ii) at increasing concentration of Pb^{II} at basic condition (pH ~12).

Table S1. Summary of peak shifts of **PyGld** in ^{1}H NMR at different conditions.

	a	b	c	d	e	f
PyGld@pH ≈ 7.0	8.06, dd	8.14, s	8.23, d	8.28, q	8.36, s	8.41, d
PyGld@ pH ~ 12	8.04, t	8.12, t	8.21, q	8.27, q	disappear	8.38, d
Pb^{II} = 250 μM	8.04, t	8.11, s	8.20, d	8.26, t	disappear	8.38, d
Pb^{II} = 500 μM	8.04, t	8.11, s	8.21, d	8.26, t	disappear	8.38, d
Pb^{II} = 750 μM	8.04, t	8.11, s	8.22, d	8.26, t	disappear	8.38, d

(d) MALDI-TOF (m/z) analysis. **PyGld**−Pb^{II} complex formation was evaluated by mass (MALDI−TOF) analysis. Mass data showed peaks at *m/z* = 656.075 and 825.116 which are corresponding to **PyGld**−Pb^{II} and **PyGld**−2Pb^{II} complexes, respectively. These results clearly confirm that **PyGld** form 1:1 complex with Pb^{II} at pH ~12, in aqueous solution. Overall, ^{1}H NMR and MALDI−TOF studies together confirmed the Pb^{II} binding to **PyGld** through gluconamide-amide deprotonation and complexation to form **PyGld**−Pb^{II} complex in basic condition.

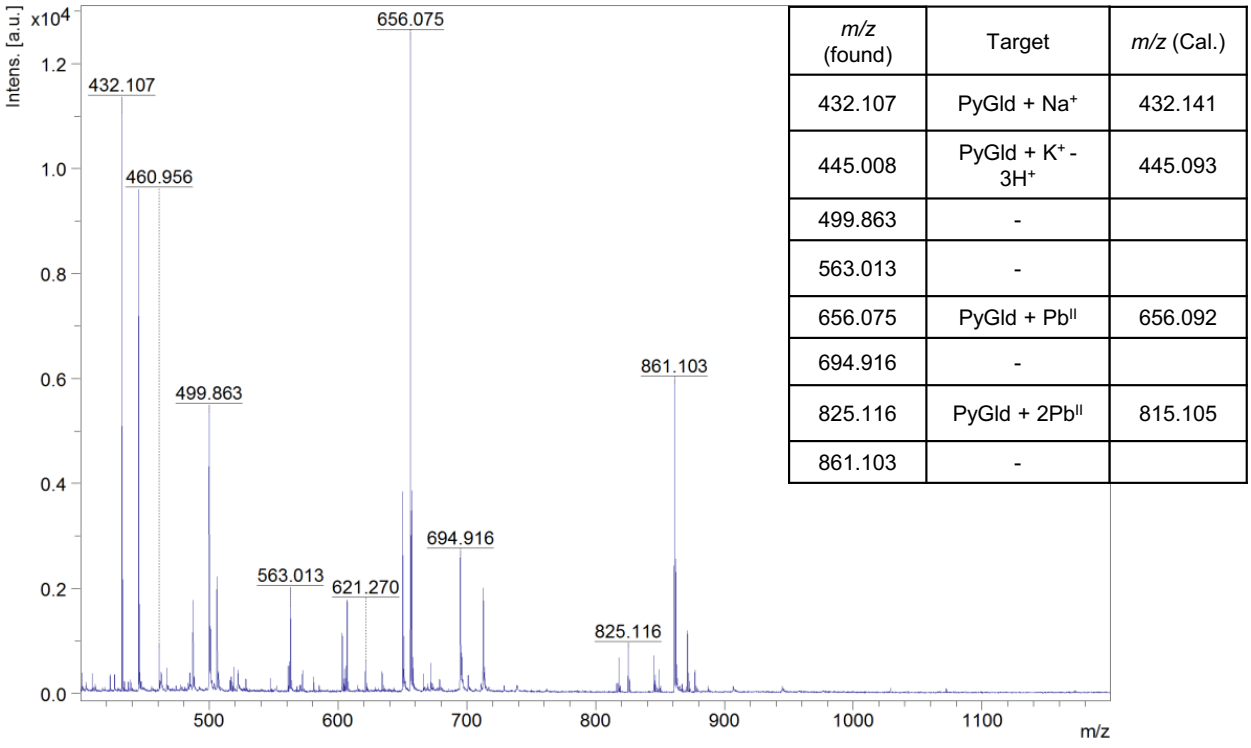

m/z (found)	Target	*m/z* (Cal.)
432.107	PyGld + Na^{+}	432.141
445.008	PyGld + K^{+} - $3H^{+}$	445.093
499.863	-	
563.013	-	
656.075	PyGld + Pb^{II}	656.092
694.916	-	
825.116	PyGld + 2Pb^{II}	815.105
861.103	-	

Figure S6. MALDI−TOF mass data of the **PyGld**−Pb^{II} complex (1:1) prepared at pH ~12 in 5%(*v/v*) DMSO−water and at 22 °C.

(e) **FTIR study.** FTIR spectra of two different sets of samples (**1**−**3** and **4**,**5**) were collected and compared with their characteristic peaks. The absorption bands of $Pb(NO_3)_2$ in aqueous (**4**) and basic condition (**5**) show peak at 3447 cm^{-1} which can be assigned to the −OH group. The peaks at 1387 and 848 cm^{-1} can be assigned to the stretching vibration or bending vibrations of the $-NO_3$ group. The absorbance spectrum of **5** shows peaks at 480, 563 and 691 cm^{-1} can be assigned to the peaks of Pb−O bond.[5,6]

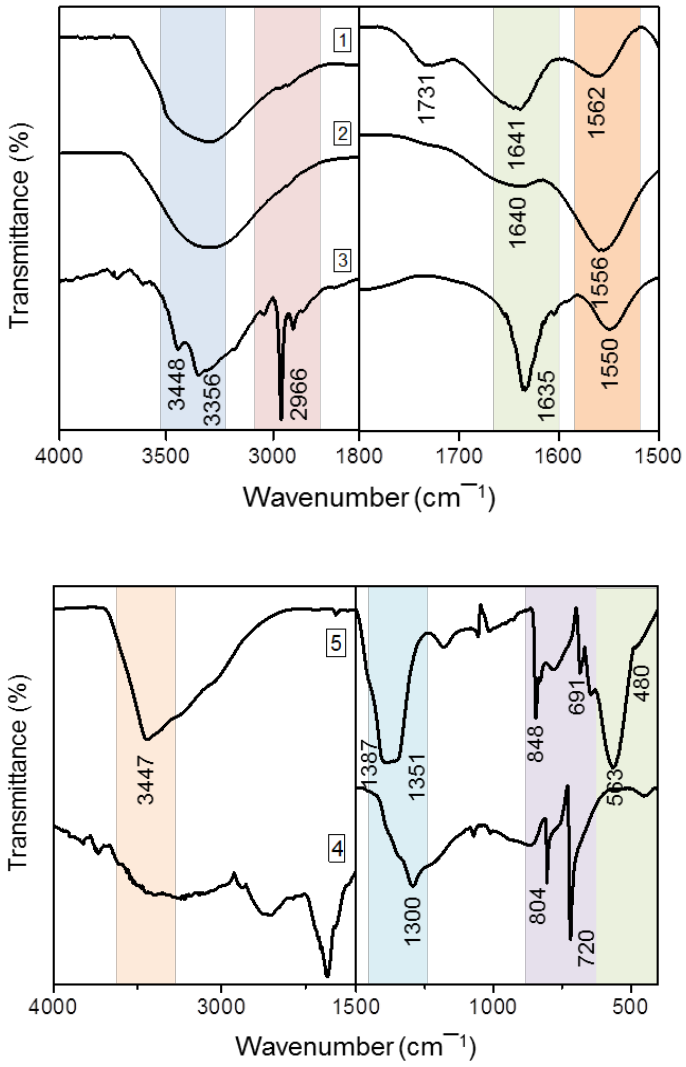

Figure S7. FTIR spectra of **PyGld** (in aqueous solution, **3**), **PyGld** (basic condition, **2**), **PyGld**-Pb^{II} complex (basic condition, **1**), $Pb(NO_3)_2$ (basic condition, **5**) and $Pb(NO_3)_2$ (aqueous solution, **4**).

(f) XPS study of PyGld and PyGld−Pb^{II}

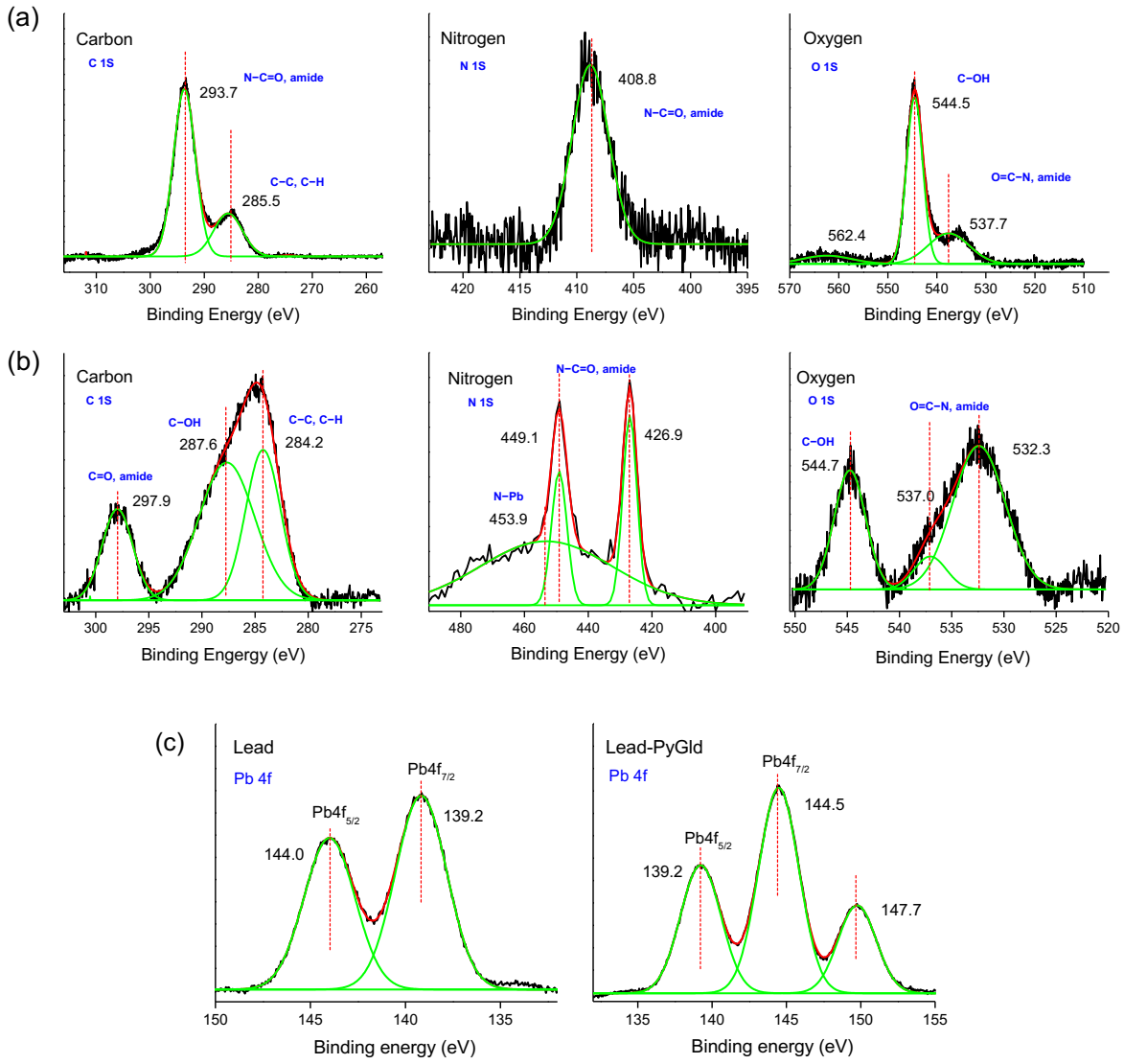

Figure S8. XPS spectra of (a) **PyGld** (aq.), (b) **PyGld**−Pb^{II} (basic condition) and (c) $Pb(NO_3)_2$ (aq.).

(g) **Powder X-ray diffraction (PXRD) Study.** Crystallinity increases with the aromatic unit in the gluconamide in the order **ProGld**<**PheGld**<**NapGld**<**PyGld**. The broad diffraction pattern for **ProGld** represents amorphous nature of the power sample.

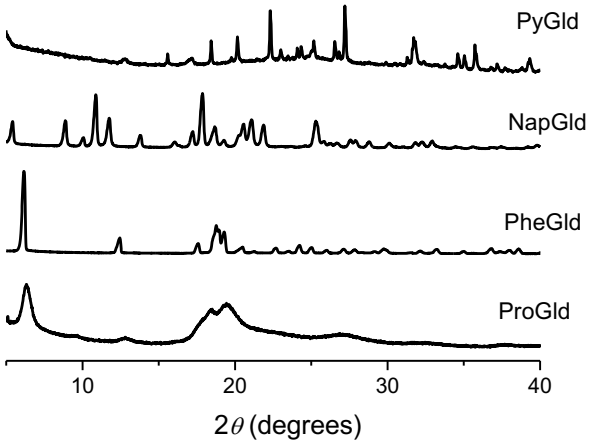

Figure S9. PXRD of the powdered samples prepared from the gluconamide−Pb^{II} complexes.

(h) Selected area diffraction (SAED) study

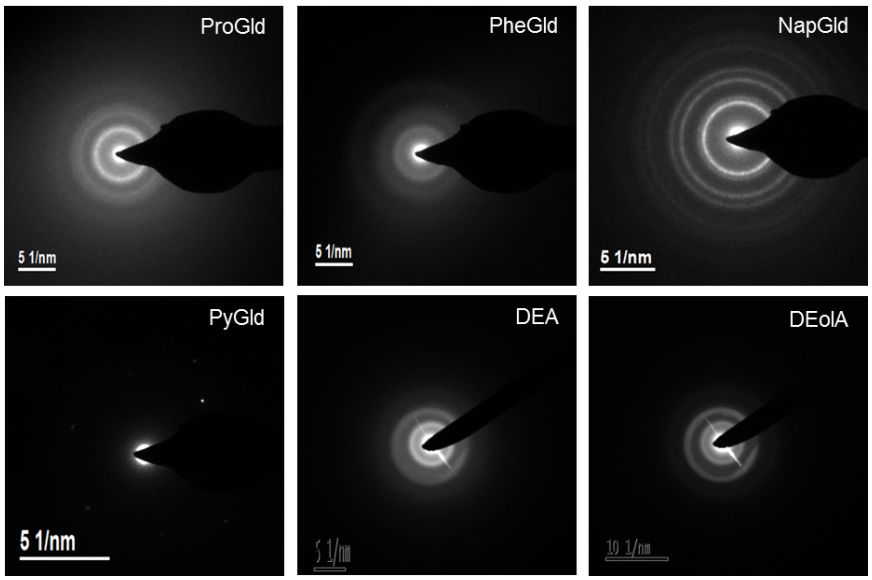

Figure S10. SAED data of different gluconamide−Pb^{II} assembly-architectures.

(j) pH responsiveness of PyGld−Pb^{II} assembly

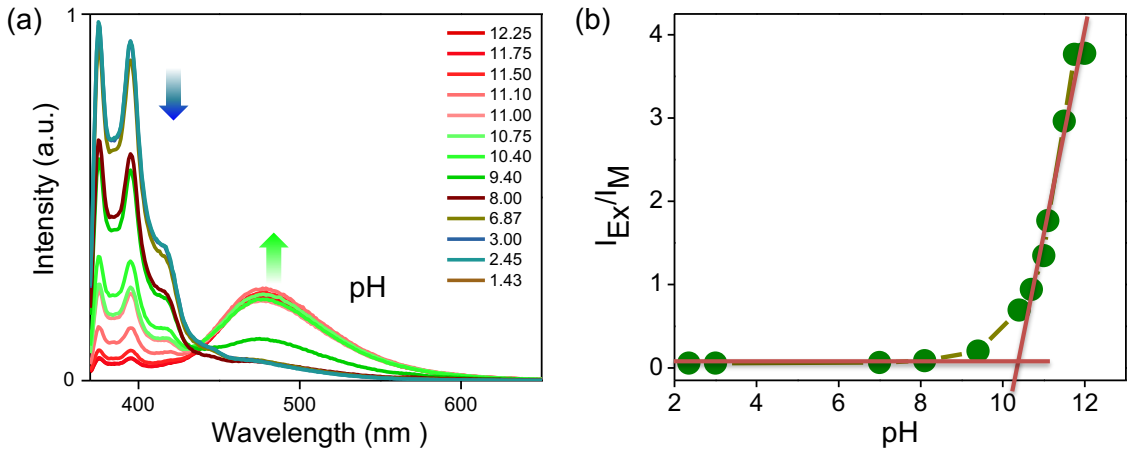

Figure S11. FL spectra (a) of **PyGld** (50 μM) in presence of Pb^{II} at different pH in 5%(*v/v*) DMSO−H_2O at 22 ºC. (b) Plot of I_{Ex}/I_M as a function of pH.

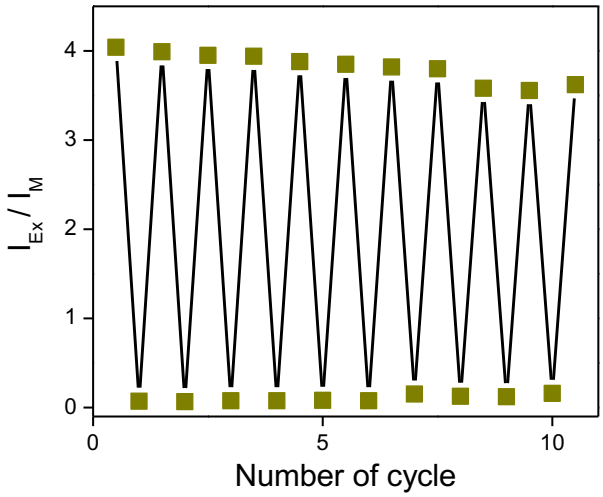

Figure S12. Fluorescence intensity ratios (I_{Ex}/I_M) are plotted against the number of cycles for **PyGld** (50 μM) in the presence of 250 μM Pb^{II} using successive additions of aq. NaOH and aq. HCl. The spectra were recorded with 1 h of aging for each state in an experiment performed over a period of one day.

(k) Mono- and disaccharide hydrolysis using PyGld−Pb^{II} assembly-architecture.

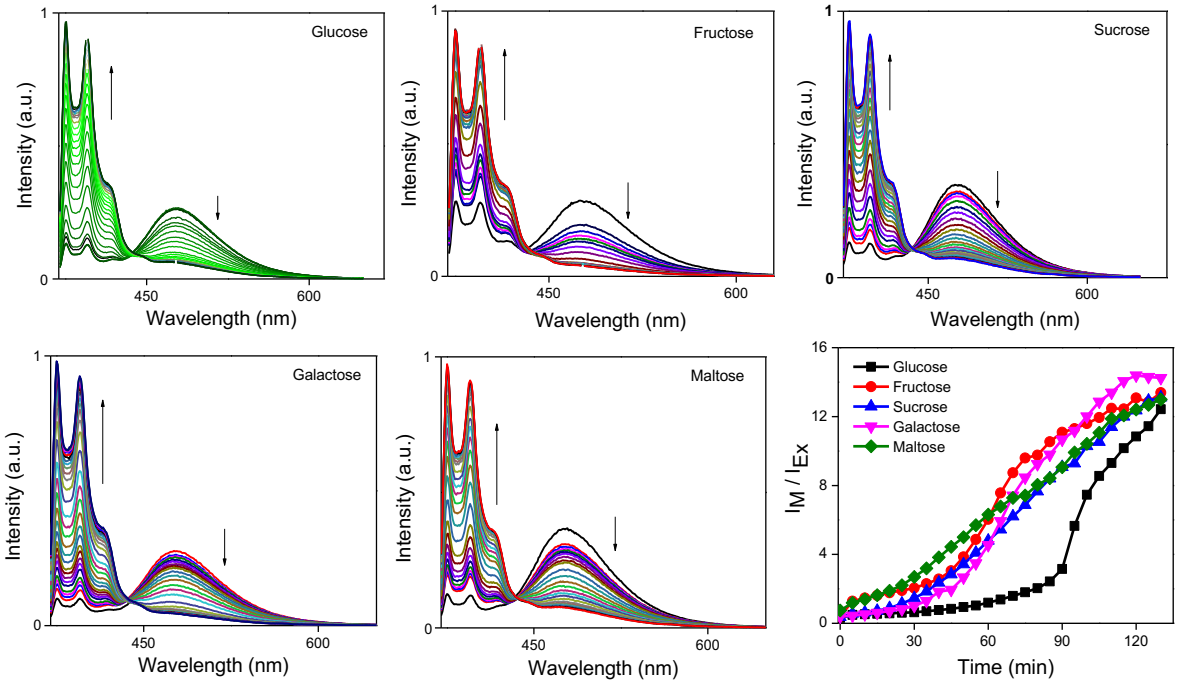

Figure S13. Change in fluorescence spectra of **PyGld**−Pb^{II} complex against time (min) in the presence of 8 mM of mono- and disaccharides. The complex was prepared by mixing 50 μM of **PyGld** and 250 μM Pb^{II} using aq. NaOH in 5%(*v/v*) DMSO−H_2O (at pH ~12).

(l) Product yield determination by quantitative NMR (Q−NMR) measuremnts. The stock solutions were prepared in DMSO−*d6* and D_2O. The catalyst mixtrue were mixed−well during the sample preparation in DMSO−D_2O (1:1, *v/v*). The solutions were aged for 2 h. Later, 8 mM glucose solution was added into the sample solution and aged for 14.5 h at 22 ºC before recording the final ^1H NMR data. The solution was filtered in a syringe filter of 0.20 μM pore size and calculated amount of sodium acetate was used as calibration compound in the Q−NMR study.

Q-NMR analysis. The mathematical formula for calculation of the amount of product formic acid (FA) formation in glucose hydrolysis is shown below. Sodium acetate was used as

calibration compound (cal) for the quantification of FA (x) formation during glucose hydrolysis. We have considered the purity of the calibration compound is 100%.

$$C_x = \frac{I_x}{I_{cal}} \times \frac{N_{cal}}{N_x} \times C_{cal}$$

I = Integral of area, N = No of nuclei, C = Concentration.

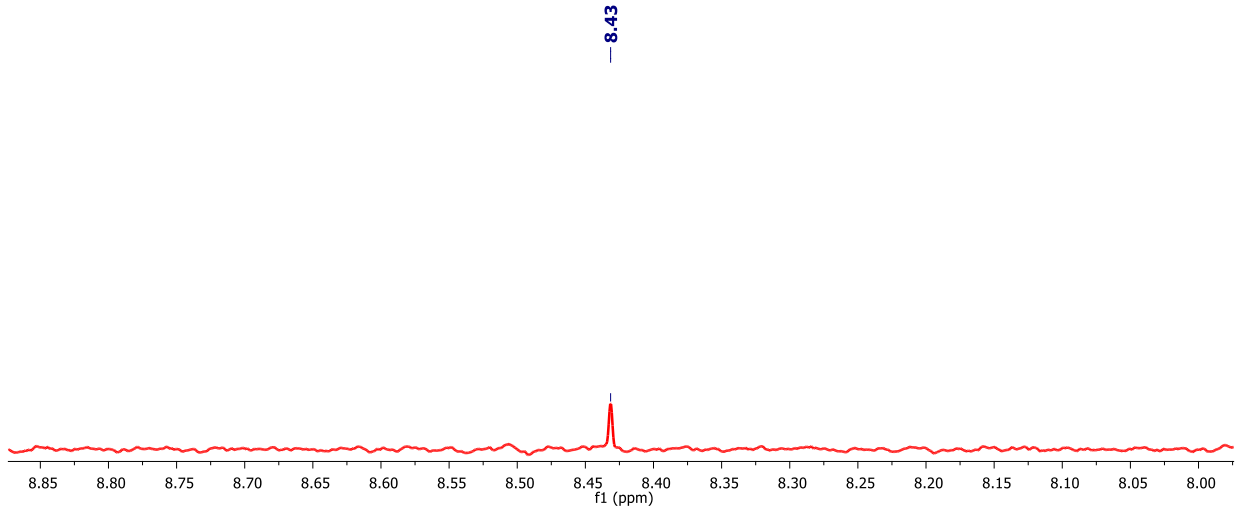

Figure S14. Q-NMR spectra of final solution in the **PyGld**-Pb^{II} in D_2O.

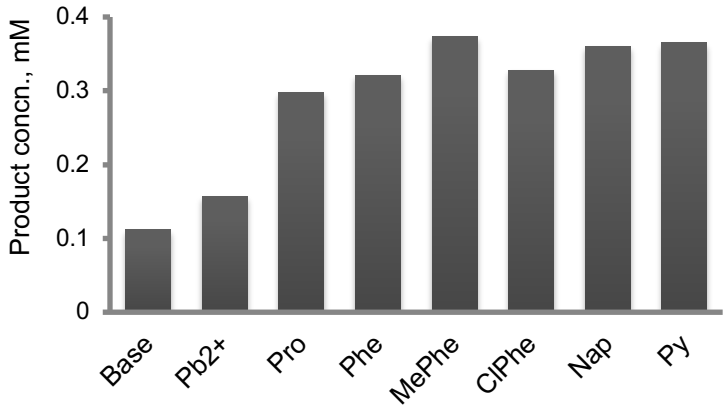

Figure S15. Yield calculation for FA formation after 14.5 h of reaction at 22 ºC. Calculated yields in percentage are 1.4%, 1.9%, 3.7 %, 4.0%, 4.7%, 4.1%, 4.5%, and 4.6%, respectively.

(m) **Concentration dependence kinetic study.**

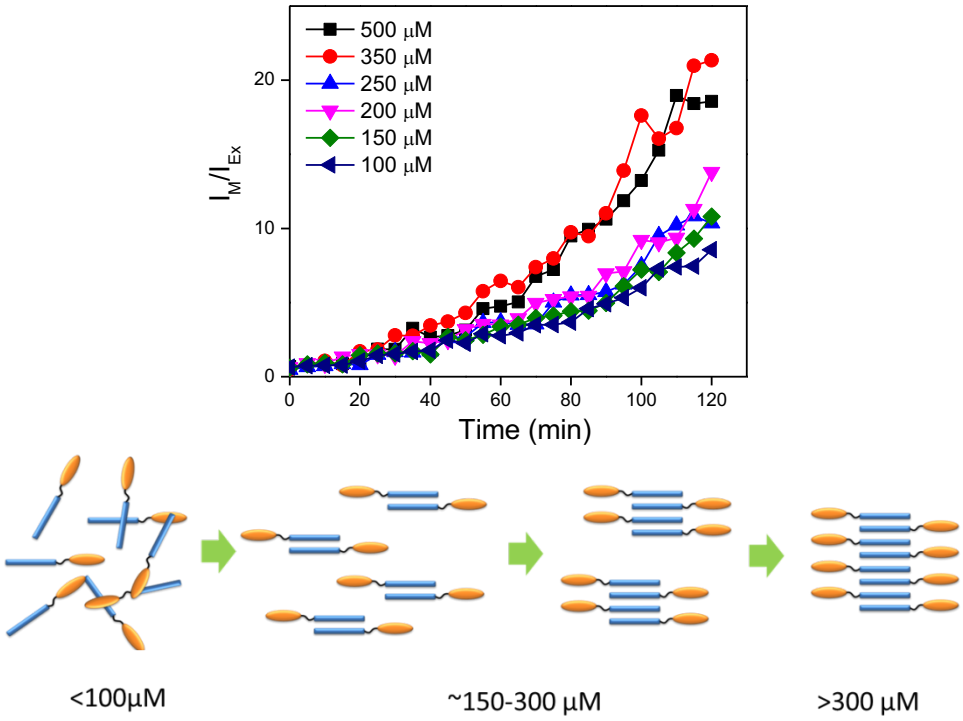

Figure S16. Kinetic study of glucose (8 mM) hydrolysis in the presence of gluconamide−Pb^{II} complexes prepared with **PyGld** (50 μM) and Pb^{II} (100−500 μM) at pH ~12 in 5%(*v*/*v*) DMSO−H_2O and 22 ºC.

(n) **Mass analysis.**

Mass spectrum of $Pb(NO_3)_2$ in water

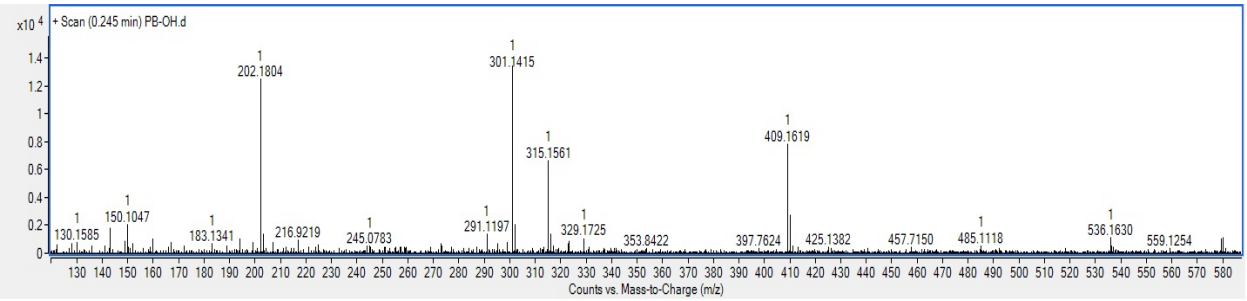

Mass spectrum of $Pb(NO_3)_2$ in base (pH ~12)

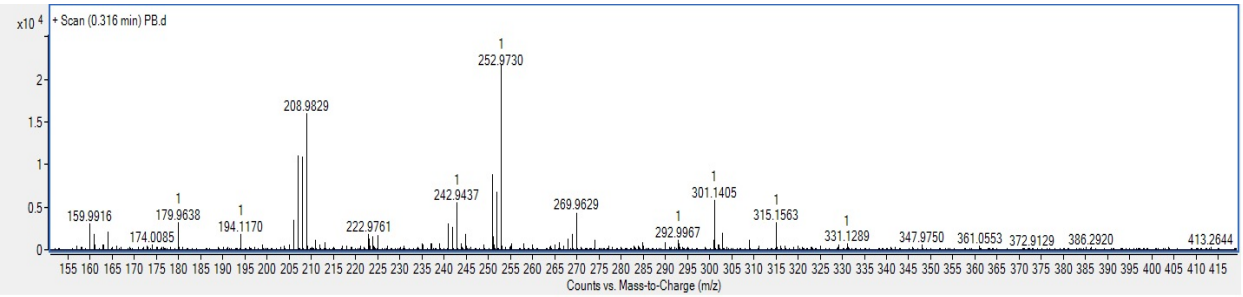

HRMS of **PyGld**-Pb^{II}

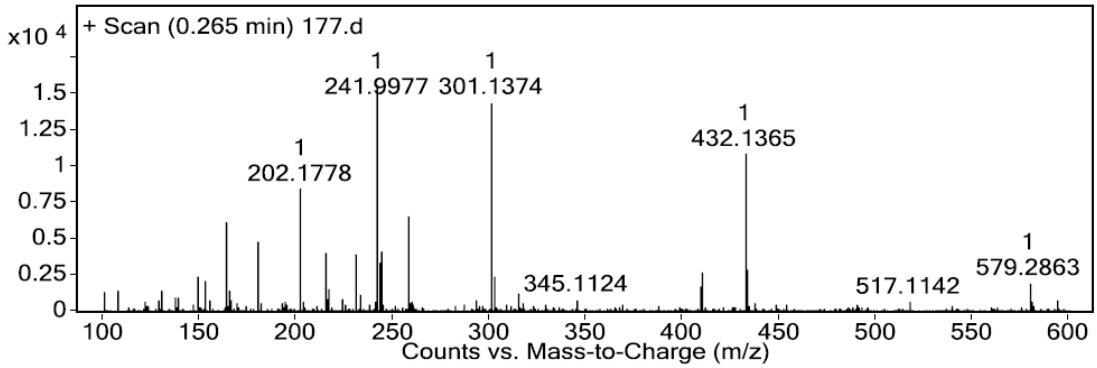

$[^{208}Pb(OH)]^+$: calculated = 224.9788; found = 224.9770
$[^{208}Pb(OH)_2]$: calculated = 241.9821; found = 241.9977
$[^{207}Pb(NO_3)]^+$: calculated = 269.9645; found = 269.9629
$[^{207}PbNO_3(OH)_2]^-$: calculated = 303.9621; found = 301.1374
[**PyGld**+Na^+−H^+]: calculated = 433.1501; found = 432.1365, 433.1393

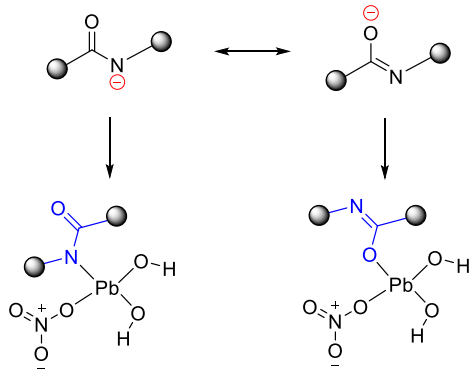

Figure S17. Mass spectra (*m/z*) of the samples. The mass data provides further evidence for the formation of different Pb^{II} species. Illustration of the different binding modes for amide−metal ion in the experimental conditions studied.

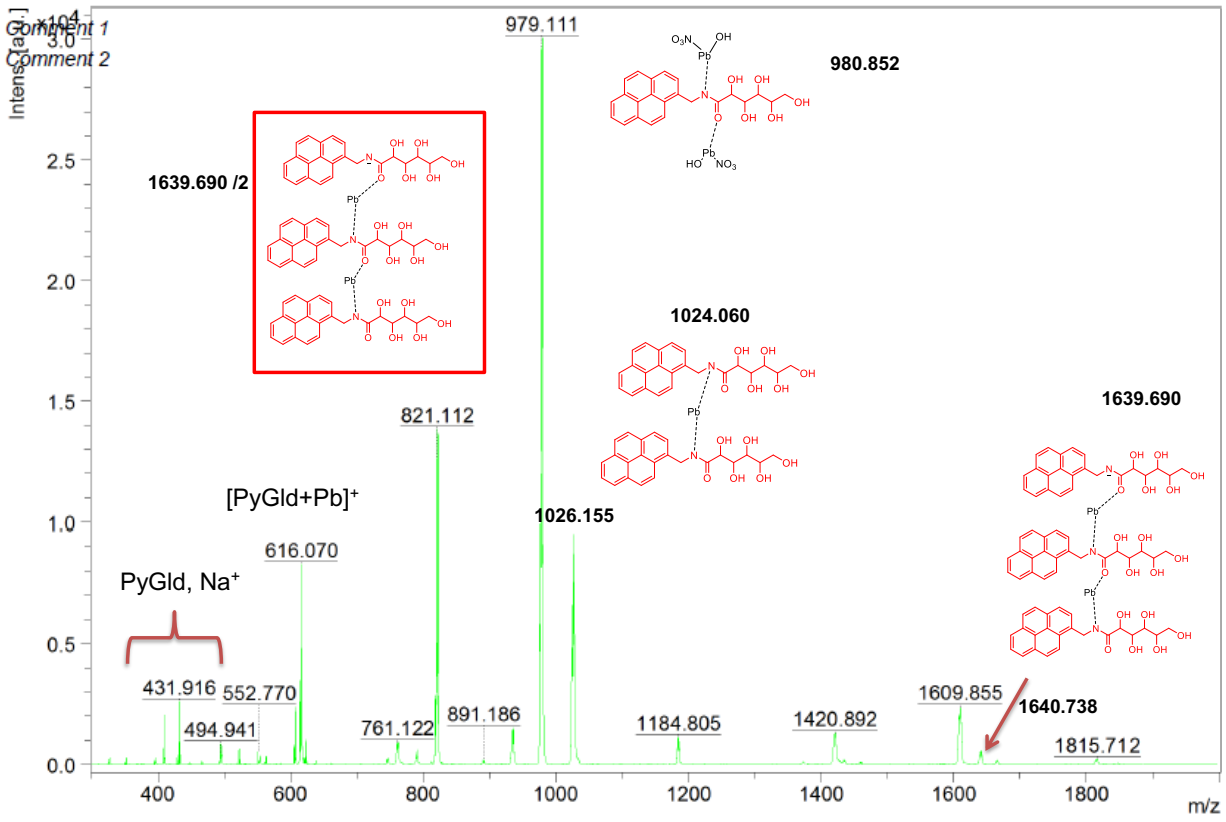

Figure S18. MALDI-TOF spectra for **PyGld**−Pb^{II} assembly-architectures. The mass data shows existence of monomer and oligomers of **PyGld** in the presence of Pb^{II} under the experimental conditions studied.

4. Reference

(1) Arévalo, M. J.; Avalos, M.; Babiano, R.; Cabanillas, A.; Cintas, P.; Jiménez, J. L.; Palacios, J. C. Optically active sugar thioamides from δ-gluconolactone. *Tetrahedron Asymmetry* **2000**, *11*, 1985-1995.

(2) Briard, J. G.; Fernandez, M.; De Luna, P.; Woo, T. K.; Ben, R. N. QSAR Accelerated Discovery of Potent Ice Recrystallization Inhibitors. *Sci. Rep.* **2016**, *6*, 26403.

(3) Piispanen, P. S.; Persson, M.; Claesson, P.; Norin, T. Surface properties of surfactants derived from natural products. Part 1: Syntheses and structure/property relationships—Solubility and emulsification. *J. Surfactants Deterg.* **2004**, *7*, 147-159.

(4) Briard, J. G.; Jahan, S.; Chandran, P.; Allan, D.; Pineault, N.; Ben, R. N. Small-Molecule Ice Recrystallization Inhibitors Improve the Post-Thaw Function of Hematopoietic Stem and Progenitor Cells. *ACS Omega* **2016**, *1*, 1010-1018.

(5) Xu, X.; Yang, B.-P.; Huang, C.; Mao, J.-G. Explorations of New Second-Order Nonlinear Optical Materials in the Ternary Rubidium Iodate System: Noncentrosymmetric β-RbIO3(HIO3)2 and Centrosymmetric Rb3(IO3)3(I2O5)(HIO3)4(H2O). *Inorg. Chem.* **2014**, *53*, 1756-1763.

(6) Wang, G.; Luo, M.; Lin, C.; Ye, N.; Zhou, Y.; Cheng, W. Lanthanum Lead Oxide Hydroxide Nitrates with a Nonlinear Optical Effect. *Inorg. Chem.* **2014**, *53*, 12584-12589.